Numerical study of resonant shallow flows past a lateral cavity: benchmarking the model with a new experimental data set

A. Navas-Montilla[1], **S. Martínez-Aranda**[2], **A. Lozano**[3], **P. García-Navarro**[2]

[1] Centro Universitario de la Defensa, Zaragoza, Spain. [2] Fluid Mechanics - LIFTEC, Universidad de Zaragoza - CSIC. [3] LIFTEC-CSIC, Zaragoza, Spain

anavas@unizar.es

1 Introduction

Steady shallow flows past an open channel lateral cavity have been widely studied in the last years due to their engineering and environmental relevance, e.g. for river restoration purposes. Such flows can induce the excitation of an eigenmode of a gravity standing wave inside the cavity, called seiche, which may be coupled with the shedding of vortices at the opening of the cavity [1] (Figure 1). This was reported to be associated with the presence of large-scale coherent vortical structures in the unstable shear layer. The presence of the seiche is of fundamental interest as it enhances the mass exchange between the main channel and the cavity [2]. Measurements of the time evolution of the water surface are scarcely reported in the literature for this type of flows [3]. In this work, we benchmark a SWE numerical model with a new experimental dataset involving surface and velocity measurements.

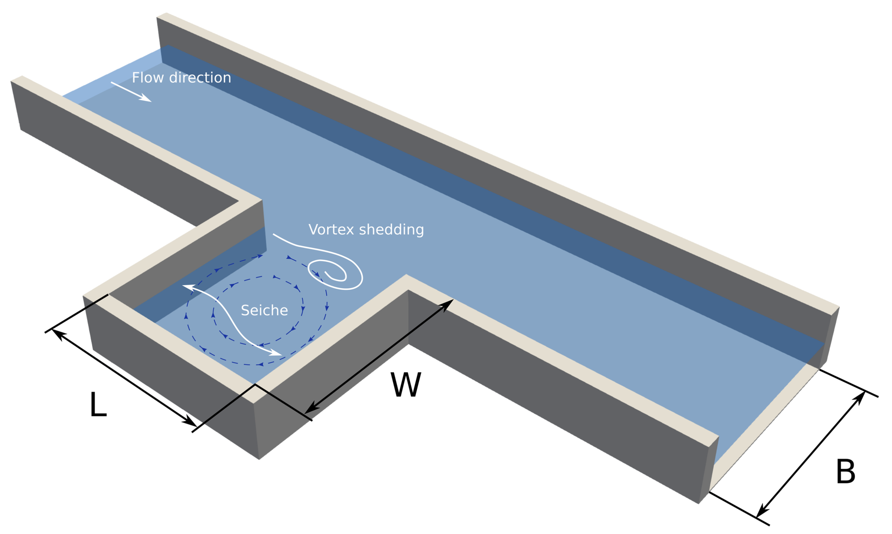

Figure 1: Typical channel-cavity flow configuration and relevant flow features.

2 Mathematical and numerical modelling

The problem can be modelled by the Shallow Water Equations (SWE) with bottom topography, friction and turbulence [4]:

$$\frac{\partial}{\partial t}\begin{pmatrix} h \\ hu \\ hv \end{pmatrix} + \frac{\partial}{\partial x}\begin{pmatrix} hu \\ hu^2+\frac{1}{2}gh^2 \\ huv \end{pmatrix} + \frac{\partial}{\partial y}\begin{pmatrix} hv \\ huv \\ hv^2+\frac{1}{2}gh^2 \end{pmatrix} = \begin{pmatrix} 0 \\ -gh\frac{dz}{dx} - c_f\,|\mathbf{v}|\,u \\ -gh\frac{dz}{dy} - c_f\,|\mathbf{v}|\,v \end{pmatrix} + \mathbf{D}, \quad (1)$$

where the source term accounts for the bed variations and friction and $\mathbf{D}$ is the diffusion term. The friction coefficient c_f is computed using the Manning formulation as $c_f = \frac{gn^2}{h^{1/3}}$. The diffusion term is computed using the Boussinesq approximation as:

$$\mathbf{D} = \frac{\partial}{\partial x}\begin{pmatrix} 0 \\ 2h(\nu+\nu_t)\partial_x u \\ h(\nu+\nu_t)(\partial_x v + \partial_y u) \end{pmatrix} + \frac{\partial}{\partial y}\begin{pmatrix} 0 \\ h(\nu+\nu_t)(\partial_x v + \partial_y u) \\ 2h(\nu+\nu_t)\partial_y u \end{pmatrix}, \quad (2)$$

where ν is the molecular viscosity and ν_t is the turbulent viscosity, computed as a sum of a vertical and a horizontal component $\nu_t = \sqrt{(\nu_t^v)^2 + (\nu_t^h)^2}$. Following the URANS methodology, we aim at: **modelling** the small-scale 3D turbulence, using $\nu_t^v = \lambda U^* h$ and **resolving** the large-scale 2D vortices, only **modelling** (via ν_t^h) the 2D unresolved scales if required [4] (WENO methods may play this role).

The SWE model above is solved using a 3-rd order WENO-ADER scheme. The motivations for using a high order scheme comprise: **a low numerical dissipation and dispersion** (a large extent of the 2D turbulence spectrum can be resolved) and **a high computational efficiency** (time and memory saving). The proposed numerical method can be written in fully-discrete form [4]:

$$\overline{\mathbf{U}}_{ij}^{n+1} = \overline{\mathbf{U}}_{ij}^{n} - \frac{\Delta t}{\Delta x^2}\left(\sum_{r=1}^{4}\mathcal{F}_r^- - \bar{\mathbf{S}}_{ij} - \bar{\mathbf{D}}_{ij}\right), \quad (3)$$

where $\bar{\mathbf{S}}_{ij}$ and $\bar{\mathbf{D}}_{ij}$ are the approximation of the the source term and diffusion term, respectively, inside the cell and $\mathcal{F}_r^-$ are the numerical fluxes.

3 Numerical results

The experimental facility consists of a free-surface open channel made of methacrylate. The channel is $6\,m$ long with a constant width rectangular cross-section of $B = 24\,cm$, with 0.25% longitudinal slope. A square lateral cavity $24 \times 24\,cm$ (width to length ratio $W/L = 1$) was placed on one side of the channel. Five different steady experiments were carried out $S6$, $S8$, $S10$, $S12$ and $S14$ with constant inflow discharges 6, 8, 10, 12, and $14\,m^3/h$ respectively. The main flow features for each case are shown in Table 1. The seiche periods, both experimental T_{exp} and analytical T_{theo}, are presented in the table.

Case	q (m^3/h)	h_u (mm)	Fr	Re	T_{exp} (s)	T_{theo} (s)	$\Delta h_{k=1}$ (mm)	$\Delta h/h_u$
S14	14	35	0.79	5018	0.77	0.82	4.29	0.123
S12	12	31	0.81	4415	0.80	0.87	4.04	0.130
S10	10	28	0.79	3754	0.84	0.92	3.53	0.126
S8	8	24	0.80	3086	0.91	0.99	3.19	0.132
S6	6	20	0.78	2381	1.00	1.08	1.72	0.086

Table 1: Case configurations. Water depths measured upstream and downstream the cavity are denoted by h_u and h_d.

Figure 2 shows the spatial distribution of the amplitude of the first oscillation mode (i.e. associated to the fundamental seiche frequency, $k = 1$) for the measured and computed water surface elevation. This representation allows to visually analyze the oscillation patterns in the region of interest (i.e. cavity and channel interaction area). A particular oscillation pattern composed of two nodes and three anti-nodes is observed along the shear line at the opening of the cavity (section A-A'), being stronger at the impingement corner ($y = 0$ and $x = 240$ mm). The strength of the seiche decreases as the discharge is reduced.

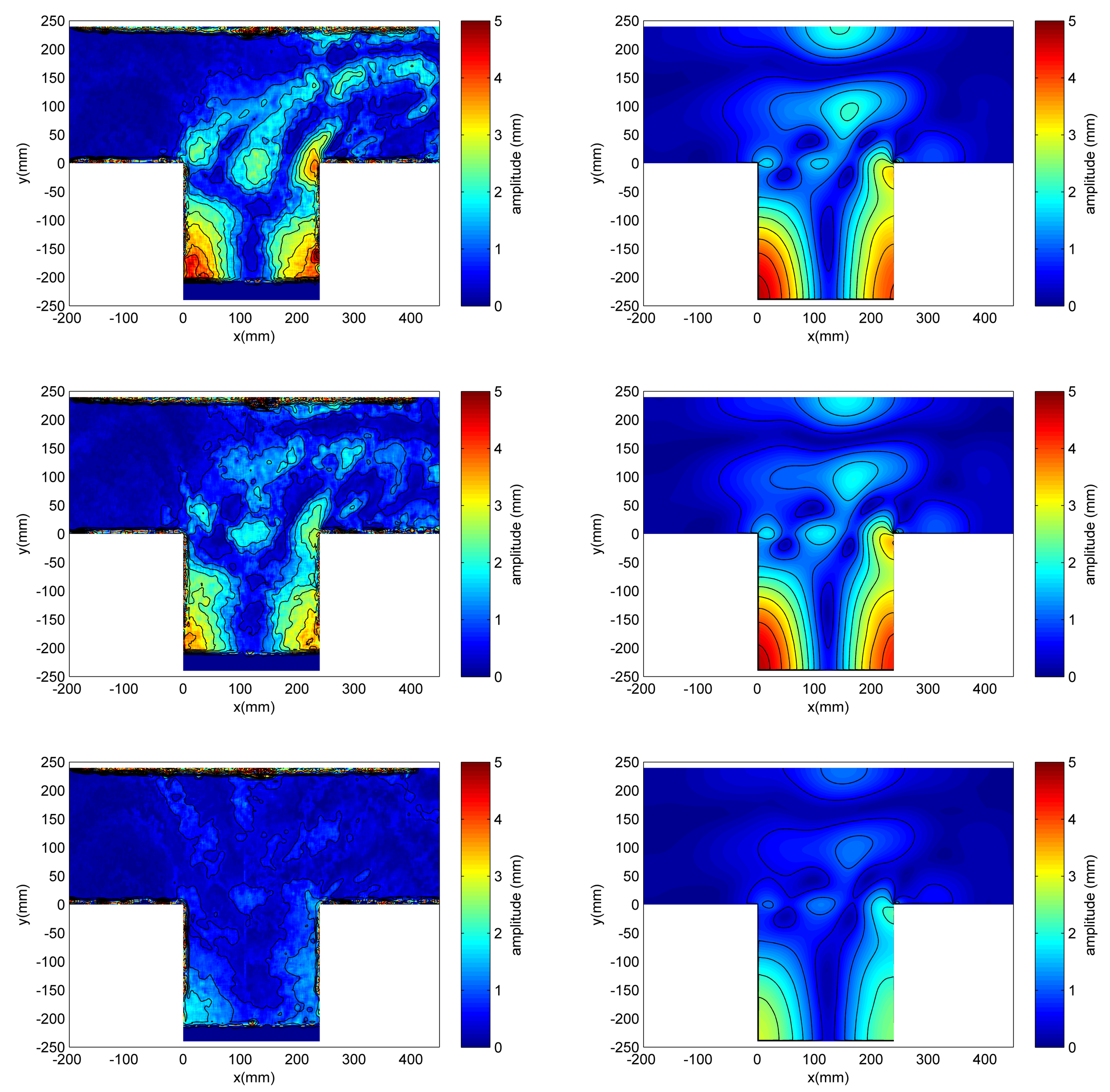

Figure 2: Experimental (left) and numerical (right) amplitude of the oscillation, measured using the first harmonic ($k = 1$). Cases S14, S10 and S6.

In order to analyze the spatial variation of the oscillation modes, the normalized power density spectrum (PSD) has been computed for case S14 (Figuree 3). It evidences that the fundamental oscillation mode is associated to the seiche, with a measured frequency that matches the theoretical estimation (Table 1). In general, no significant secondary oscillation modes are observed in the experimental and numerical data.

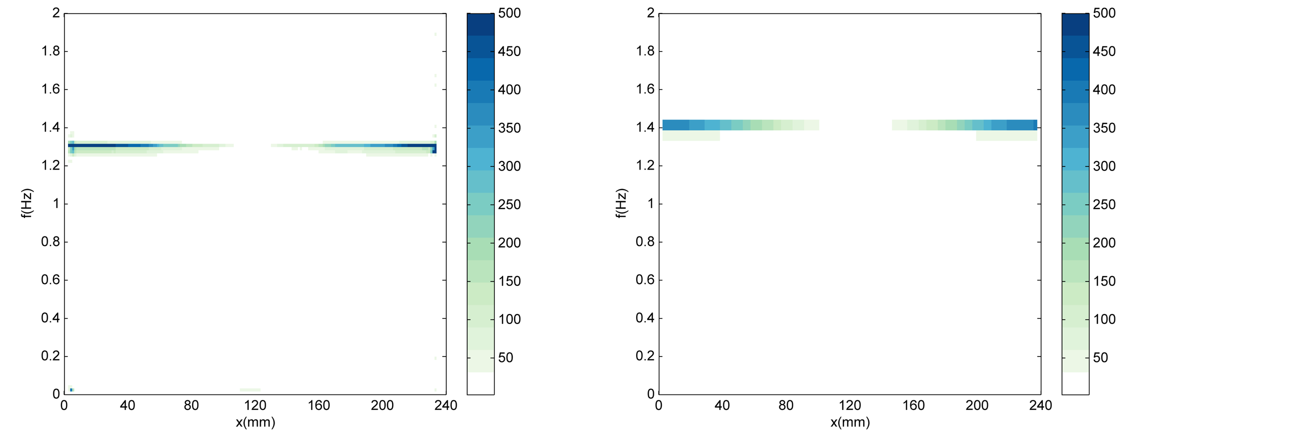

Figure 3: Case S14.Normalized power density spectrum of the measured (left) and computed (right) water surface elevation along the streamwise direction inside the cavity on the cavity innermost region.

Figure 4 shows the X and Y components, respectively, of the time-averaged velocity at the channel-cavity region for the case S14. The numerical data are compared with PIV measurements. The numerical model predicts the measured flow pattern. In general, the numerical method slightly overestimates the depth averaged velocity of the flow.

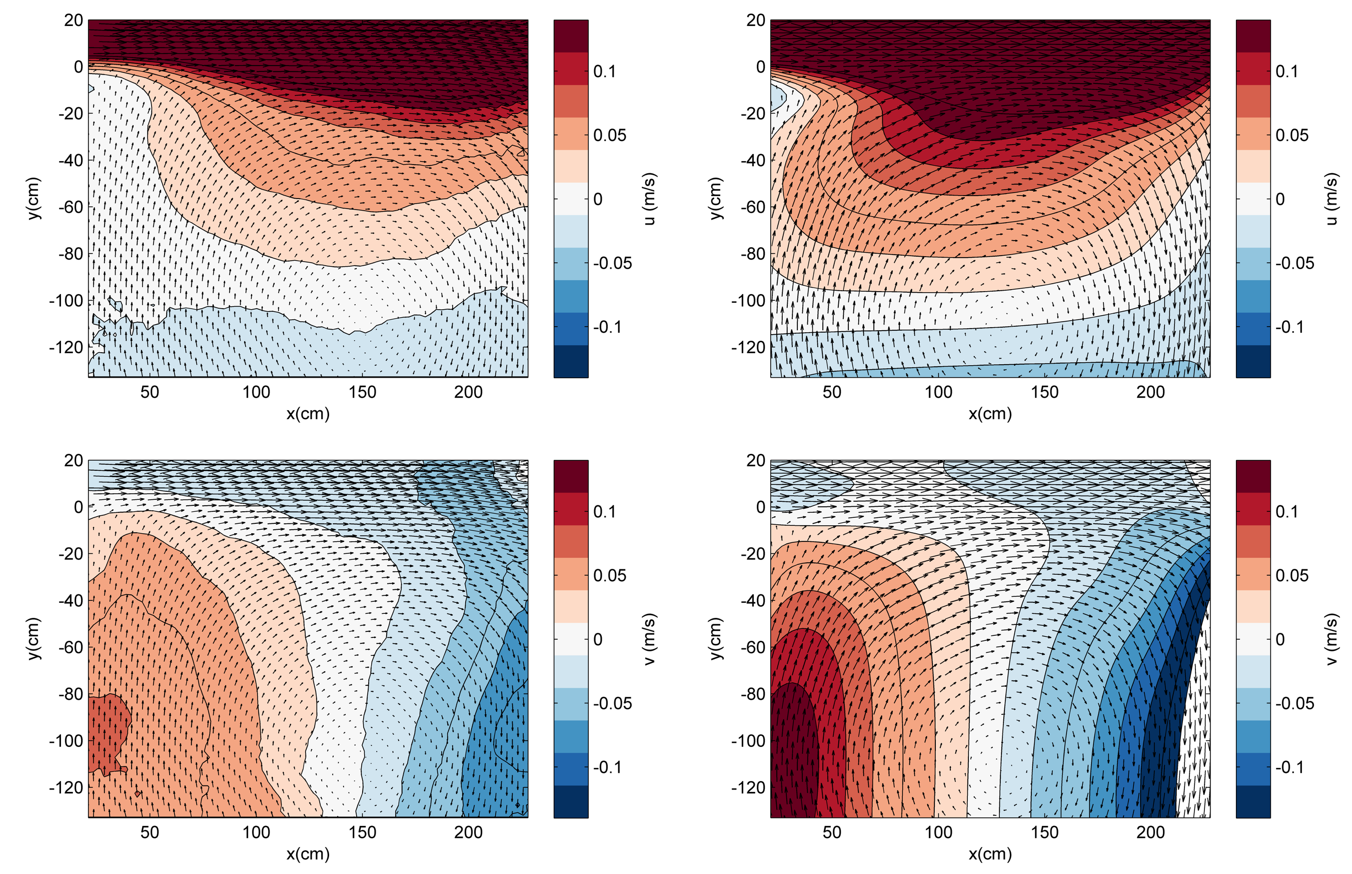

Figure 4: Case S14. Experimental (left) and numerical (right) time-averaged streamwise component of the velocity, u, (top) and spanwise component of the velocity, v, (bottom) inside the PIV measuring area.

References

[1] I. Kimura, T. Hosoda, Fundamental properties of flows in open channels with dead zone, Journal of Hydraulic Engineering 123 (1997) 98–107.

[2] Juez, C., Bühlmann, I., Maechler, G., Schleiss, A. J., Franca, M. J., Transport of suspended sediments under the influence of bank macro-roughness, Earth Surface Processes and Landforms, 43 (2018) 271–284.

[3] Engelen, L., Creëlle, S., Schindfessel, L., De Mulder, T., Spatio-temporal image-based parametric water surface reconstruction: a novel methodology based on refraction. Measurement Science and Technology, 29 (2018) 035302.

[4] Navas-Montilla A., Juez, C., Franca, M.J. and Murillo, J., Depth-averaged unsteady RANS simulation of resonant shallow flows in lateral cavities using augmented WENO-ADER schemes, Journal of Computational Physics, 24 (2019) 203–217.